Journal of Thermal Science Vol.21, No.5 (2012) 404–412

DOI: 10.1007/s11630-012-0561-2 **Article ID: 1003-2169(2012)05-0404-09**

Turbine Blade Boundary Layer Separation Suppression via Synthetic Jet: an Experimental and Numerical Study

Bernardini, C.[1], Carnevale, M.[1], Manna, M. [2], Martelli, F.[1], Simoni, D.[3], Zunino, P.

1. Università degli Studi di Firenze, Firenze, Italy
2. Università degli Studi di Napoli Federico II, Napoli, Italy
3. Università degli Studi di Genova, Genova, Italy

The present paper focuses on the analysis of a synthetic jet device (with a zero net massflow rate) on a separated boundary layer. Separation has been obtained on a flat plate installed within a converging-diverging test section specifically designed to attain a local velocity distribution typical of a high-lift LPT blade. Both experimental and numerical investigations have been carried out. Unsteady RANS results have been compared with experiments in terms of time-averaged velocity and turbulence intensity distributions. Two different Reynolds number cases have been investigated, namely Re = 200,000 and Re = 70,000, which characterize low-pressure turbine operating conditions during take-off/landing and cruise. A range of synthetic jet aerodynamic parameters (Strouhal number and blowing ratio) has been tested in order to analyze the features of control – separated boundary layer interaction for the aforementioned Reynolds numbers.

Keywords: Synthetic Jet, Separated Flow, Active Flow Control, Unsteady Flow, Ultra High Lift LPT.

Introduction

Environmental and economic concerns are the leading themes for modern aero jet-engine design. Low pressure turbines (LPT) are subjected to a wide range of Reynolds numbers from typical values of ~10^6 at sea level, down to very low values (below 10^5) associated with high altitude which may induce massive flow separation and finally dramatic loss increase. When transition from laminar to turbulent flow does not occur due to the low Reynolds number, boundary layer separation usually appears on the suction side. In these conditions control of boundary layer development is a promising strategy to obtain performance improvement. Passive and active devices are commonly adopted technologies for this purpose. The synthetic jet (SJ) is a zero-net massflow active control device which is meant to re-energize the boundary layer through a repeated sequence of suction and blowing phases in order to make it more resistant to the adverse pressure gradient. In the suction phase high-momentum fluid from outside the boundary layer is drawn toward the wall, while in the blowing phase high-energy flow is directly introduced inside the boundary layer. SJ has been proven to be an effective technology for loss reduction by means of separation suppression (Honoan *et al.* [1]) in particular on airfoils (You *et al.* [2]) and LPT blades (Volino [3]). This technique has the neat advantage that it does not need additional air flow spill from the compressor. The zero net massflow process occurs through a slot on the suction side usually just upstream of separation and it is expected to trigger boundary layer transition. Although several studies with active and

Received: July 2012
C. Bernardini: Ph.D..

Nomenclature

C_f	skin friction coefficient	T	jet period
C_p	pressure coefficient $=\frac{p_{tin}-p}{p_{tin}-p_{in}}$	Tu	turbulence intensity
C_μ	jet momentum coefficient	u	streamwise velocity
f_{act}	actuator frequency	U_{in}	Inlet streamwise velocity magnitude
L	flat plate length	U_{act}	maximum outstroke velocity
L_{sep}	streamwise separation length	x	streamwise coordinate
p	static pressure	x_{sep}	streamwise separation onset coordinate
p_t	total pressure	y	normal to the wall coordinate
r	jet to main flow velocity ratio $=\frac{U_{act}}{U_{in}}$	ν	kinematic viscosity
Re	isentropic inlet Reynolds number=$U_{in}L/\nu$	ρ	density
St	jet Strouhal number $=\frac{f_{act}L}{U_{in}}$		

passive control have been undertaken on high-lift profiles (Vera *et al.* [4] , Rizzetta *et al.* [5]), SJ effectiveness on real high-lift LPT profiles has not been largely addressed. This paper aims at investigating the capability of such device to suppress boundary layer separation in high-lift LPT conditions by adjusting its control parameters at different Reynolds numbers.

As the field of active flow control has seen a significant growth over the last decade, the need for accurate computational predictive tools becomes more and more pressing. Many methodologies are available for engineers, ranging from fast and relatively inexpensive methods with a significant amount of modelling such as Unsteady Reynolds Averaged Navier-Stokes (URANS), to time consuming methods with high flow resolution such as Large-Eddy Simulation or Direct Numerical Simulation. Currently, since the latter kind is too time- and CPU-consuming for most practical applications URANS remains the most viable tool. A large literature addressing the performance of URANS computations for active flow control applications is available (Rumsey *et al.* [6], Dejoan *et al.* [7]). However, in these works the boundary layer was subject to zero or very low adverse pressure gradient. The main outcome of these studies is the ability of the eddy viscosity models to predict the qualitative behaviour of the unsteady forced interaction between jet and boundary layer. This allows to correctly defining trends with control parameters (Bernardini *et al.* [8]). Nevertheless, quantitative errors occur, which are mainly due to the adopted turbulence. In the present paper the performance of a three equation turbulence/transition model is investigated while attempting to reproduce experimental data, in order to assess the potential of URANS simulations to predict synthetic jet effects with a strong adverse pressure gradient.

Simulations have been carried out by University of Firenze and Napoli research groups while experimental results have been undertaken by the University of Genova.

Experimental Facility and Measuring Techniques

Experiments have been performed in the open loop low speed wind tunnel installed in the Laboratory of Aerodynamics and Turbomachinery of the University of Genova. As shown on Fig.1, the test section consists of a thick flat plate with (8:1) elliptic leading edge and a sharp trailing edge. The flat part of the plate, including the leading edge, is 200 mm long and 300 mm wide. The plate has been installed between two contoured walls that produce the prescribed adverse pressure gradient, typical of high-lift turbine blades.

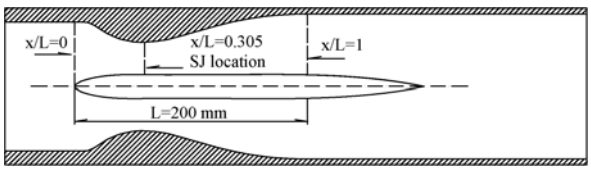

Fig.1 Schematic of test section.

A rectangular slot, 0.5 mm wide and 200 mm long, cuts the plate surface at 60 mm from the plate leading edge. The synthetic jet is generated by means of a reciprocating system (15 cm^3 displacement) connected to the cavity placed inside the plate, as shown in Fig. 2 (adopting a configuration similar to that proposed by Gilarranz and Rediniotis [9]).

The cavity within the plate, which almost extends along the whole length and width of the plate, has been connected to the piston system by a set of 6 pipes, 3 for

each side, to ensure two-dimensional jet features at midspan of the exit slot. The slot dimensions as well as piston frequencies have been chosen in order to produce the desired jet aerodynamic parameters listed in Table 1.

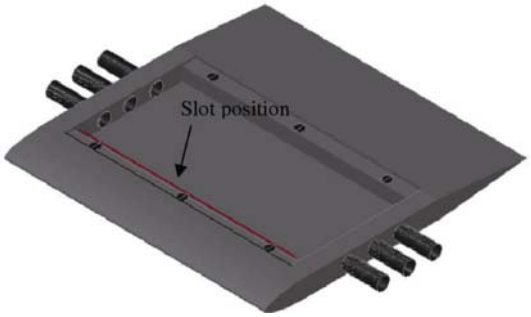

Fig.2 Geometrical configuration of the SJ cavity within the plate.

Table 1 Synthetic jet non-dimensional parameters

St	r	C_μ
0.25	0.29	$4.3\ 10^{-4}$
0.5	0.59	$1.7\ 10^{-3}$
1	1.18	$6.9\ 10^{-3}$

The flat plate has been instrumented at flat plate midspan, downstream of the velocity peak position, with a total of 25 pressure taps connected to a Scanivalve. Static pressure was measured by means of high-sensitiveity high-accuracy low-range capacity differential transducers (SETRA). The instrument accuracy is better than ±0.075% of the transducer full-scale range (±620 Pa). This returns a pressure coefficient uncertainty which is smaller than ± 1%.

The boundary layer developing along the rear part of the plate was surveyed by means of 25 traverses (from x/L = 0.305 up to x/L = 1.0). Each traverse consisted of 31 data points collected along the normal to the wall direction, with smaller spacing close to the wall. A three-axis computer controlled traversing mechanism with a minimum linear translation step of 8 μm has been employed to allow high precision movement and an adequate spatial resolution.

A single-sensor miniature boundary layer hot-wire probe (DANTEC 55P15) has been employed for these measurements. The anemometer output voltages were sampled using a Metrabyte DAS 58 sample and hold AD converter board. As it is well known, flow direction in a separation bubble cannot be determined with a single sensor hot-wire, but velocity magnitude can be measured and it was found to be very low and nearly constant within the bubbles investigated in the present study.

At each point 140,000 samples have been collected with a sampling frequency of 20 kHz. An antialiasing low-pass filter set at 10 kHz has been adopted. Considering a 95% confidence level, the uncertainty in the velocity measurements has been evaluated to be better than 2%.

Experiments have been carried out at two Reynolds numbers based on flat plate length and inlet velocity, namely 70,000 and 200,000. The test section inlet turbulence intensity is nearly constant and is equal to 1.5% two plate lengths upstream of the leading edge. Measurements have been carried out for the steady uncontrolled condition and then with the synthetic jet operating.

Numerical Methods and Validation

Simulations have been performed in order to analyze the boundary layer development and results are compared with available experiments.

The interaction between large scale turbulence and unsteady forced perturbation is a paramount issue in controlled flow. There is some evidence in the available literature that URANS models may yield satisfactory results in predicting separated flow controlled separation mainly when the separation mechanism is related to large scale vortical structures (Dejoan *et al.* [7]).

The computational domain was built to match the experimental set-up as closely as possible. This includes a tripping device on the upper wall just after the channel throat to trigger transition and avoid, or at least decrease, upper separation. Calculations have been performed on a two-dimensional unstructured hybrid mesh, its features obeying turbulence models constraints on both the lower and upper wall. At least 20 prismatic layers are fitted in the boundary layer, whereas a first-node y^+ value much smaller than 1 everywhere, and the rest of the domain is filled up with triangular elements. Grid refinement has been performed in the jet zone. Numerical results have been obtained with finite-volume pressure based unsteady RANS solver. Spatial gradients are reconstructed by means of least square cell based method. Momentum equation fluxes are discretized with a second order upwind scheme. Time advancement is carried out with a second order implicit scheme.

Preliminarily a grid convergence study on a set of four different grids has been performed. The resulting time-averaged skin friction coefficient C_f distributions are plotted in Fig. 3. Grid 1 and 2 show some lack of accuracy in the first half of the flat plate, as observed in the peaks of C_f. Grid 3 provides results nearly identical to those of Grid 4 and therefore it has been retained for all calculations.

In order to cope with the transitional behavior of the boundary layer, transitional models are used in conjunction with turbulence ones. Two well known models are the SST+γ-Re_θ [10,11] and the k-kL-ω [12] model which have been compared in the uncontrolled case at Re =

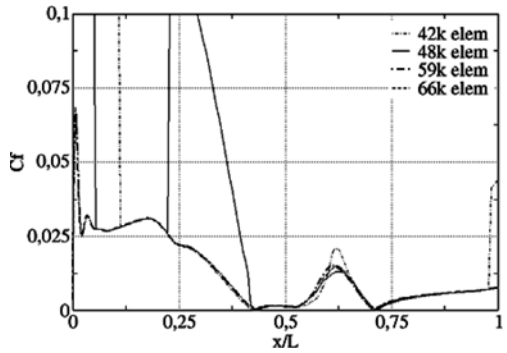

Fig. 3 Grid convergence study: mean skin friction coefficient at Re = 70,000.

70,000. The SST+γ-Re_θ model of Menter *et al.* [10] is based on the coupling of the standard SST k-ω equations with an extra equation for the intermittency function γ and one related to transition onset, in terms of momentum-thickness Reynolds number Re_θ. The k-k_L-ω model introduced by Walters and Cokljat [12] is a three-equation eddy viscosity type model, which includes transport equations for turbulence kinetic energy k, laminar kinetic energy k_L and the specific dissipation rate ω. This turbulence model also accounts for transition because the transport equation for the laminar kinetic energy which represents the energy of pre-transitional fluctuations is solved for. The resulting pressure coefficient distributions are presented in Fig. 4 together with the experimental data. The k-k_L-ω model (continuous line) appears to perform better than the SST+γ-Re_θ as it fits experimental C_p distribution for 60% of the flat plate length. Differences in the rear part of the plate should be associated with the upper wall boundary layer development discrepancies. This point will be further investigated later on in the results section. Having assessed the presence of a separation bubble in the adverse pressure gradient region of the flat plate boundary layer, the synthetic jet device has been introduced to exploit its efficiency in suppressing separation.

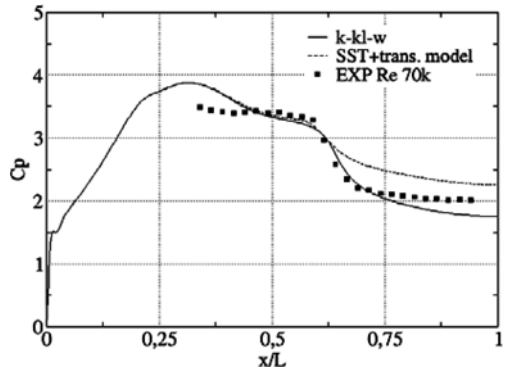

Fig. 4 Wall pressure coefficient distribution for transition models analysis.

Results and Discussions

Uncontrolled condition

The static pressure coefficient (C_p) distributions obtained along the flat plate and the top contoured wall are illustrated in Fig. 5 and Fig. 6 for Re =70,000 and Re = 200,000, respectively. For the lower Reynolds number a large laminar separation bubble can be recognized in both experimental and numerical results, as suggested by the C_p plateau at $x/L \approx 0.55$. Experiments reveal that boundary layer separation starts at $x/L \approx 0.39$, while reattachment seems to be completed only at $x/L \approx 0.69$, as detailed in Table 2. In the calculations the position of separation onset appears to be delayed, a phenomenon that could be partially attributed to the transition model. The spatial development along the upper wall as predicted by the computations differs from the experimental one, that is to say, the equivalent channel height or the streamline curvatures differ. While this is understandable downstream the throat because of the occurrence of transition and separation, it is more difficult to be accepted in the accelerating part. The separation length as predicted by the simulations is however very close to the experimental value. A bubble of shorter size takes place also along the top contoured wall. The kink in the numerical pressure coefficient distribution at x/L = 0.33 highlights the presence of the tripping device, modeled as a rectangular body, 0.2 mm high and 1 mm wide. The body is representative of an adhesive tape strip glued on the upper wall in the experimental setup. While some differences in the geometry of the two devices certainly exist, their effectiveness as boundary layer abrupt transition promotion elements may bear no resemblance at all. The main reason for these mismatches can be ascribed to the inherent approximations embodied in the transition and turbulence closure, especially at low Reynolds number.

Increasing the Reynolds number up to 200,000 reduces the size of the lower wall laminar separation bubble, as suggested by the C_p plateau length reduction visible in Fig. 6. Numerical results follow more closely the

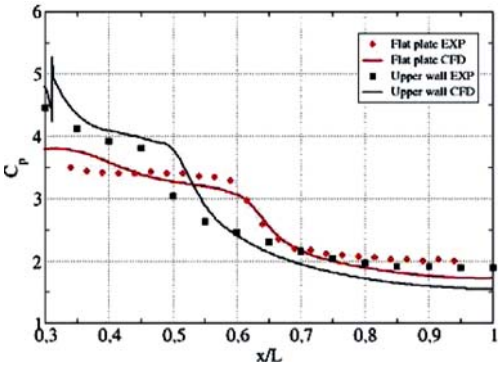

Fig. 5 Pressure coefficient distributions: Re = 70,000.

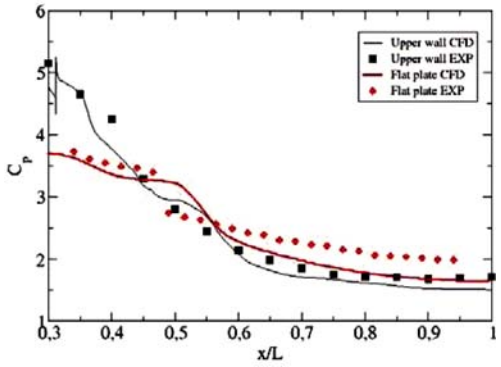

Fig. 6 Pressure coefficient distributions: Re = 200,000.

experimental trend. Actually experiments show no impact of the Reynolds number on the separation onset, while reattachment occurs sensibly upstream ($x/L \approx 0.49$).

This trend is well predicted by the calculations. On a general ground, while appreciable improvements in the separation prediction with increasing Reynolds number follow, its precise estimation is still not within reach of eddy viscosity closures. In particular, the adopted three-equation model experiences some difficulties in predicting the correct turbulent quantities spatial development in boundary layers subject to strong adverse pressure gradient (see for instance Fig. 20 of Ref. [13]). It is worth noting that the correct prediction of the lower wall separation induced transition entails an accurate prediction of the upper wall transitional boundary layer development because of the inherent non-linear (unsteady) interaction between the two boundary layers.

The laminar separation bubble structure can be observed by means of the time-averaged non-dimensional velocity contour plots illustrated in Fig.7 and Fig.8 for Re = 70,000 and Re = 200,000, respectively. For the sake of the appropriate comparison with the hot-wire measurements, the absolute value of computed streamwise velocity is reported.

Experimental velocity contours obtained at Re = 70,000 show that boundary layer separation, loosely defined by the dark blue area, occurs at around $x/L \approx 0.39$, coherently with the C_p distribution. The bubble maximum displacement position appears to be located at $x/L \approx$

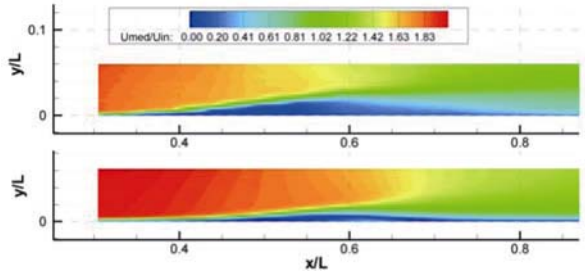

Fig. 7 U/U_{in} Velocity colour plots, Re = 70,000: experiments (top), calculations (bottom).

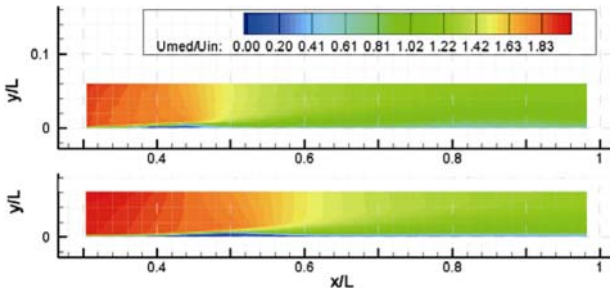

Fig. 8 U/U_{in} velocity colour plots, Re = 200,000: experiments (top), calculations (bottom).

0.58, in good agreement with the position associated with the C_p rapid slope change. At this position the bubble maximum thickness experimentally measured is $y/L \approx 0.02$. In the calculations, the maximum displacement position is rather similar ($x/L \approx 0.6$), although the bubble thickness is reduced by more than a half ($y/L \approx 0.007$). In the experiments the boundary layer time-mean reattachment occurs at about $x/L \approx 0.69$, where the velocity defect close to the wall vanishes.

For the highest Reynolds number (Re = 200,000, Fig. 8) the experimental and numerical results show a quite thin and short separated area. Using the above mentioned assumption, it may be argued that boundary layer separation occurs again at $x/L \approx 0.39$ while the maximum thickness of the bubble ($y/L \approx 0.003$) is located at $x/L \approx 0.46$, very close to the recovery position shown in the C_p distribution. The vanishing of the light blue region close to the wall confirms that the boundary layer reattaches downstream of $x/L \approx 0.49$. The numerical data again indicate that the separation bubble is longer, and the reattachment occurs at $x/L \approx 0.59$. The position of maximum displacement and its height are $x/L \approx 0.49$ and $y/L \approx 0.003$, respectively. The bubble thickness is comparable to the experimental one. Thus the main features of the separation bubble as predicted by the computations are similar to the experimental ones. Velocity and turbulence intensity profiles obtained along the rear part of the plate are shown in non-dimensional form in Fig. 9 for Re = 70,000 case, where the larger and thicker separated region has been encountered.

Boundary layer separation occurs between x/L = 0.34 and x/L = 0.44, as previously observed while discussing Fig. 7. The boundary layer transition process can be described looking at the turbulence intensity profiles. Experiments reveal that the transition process starts on the separated shear layer just over the bubble, as suggested by the local increase of the turbulence intensity in the region corresponding to the separated shear layer (see velocity profiles) from x/L = 0.34 up to x/L = 0.54. At x/L = 0.54 and y/L = 0.022 velocity fluctuations in the shear layer reach their maximum value as a consequence of the

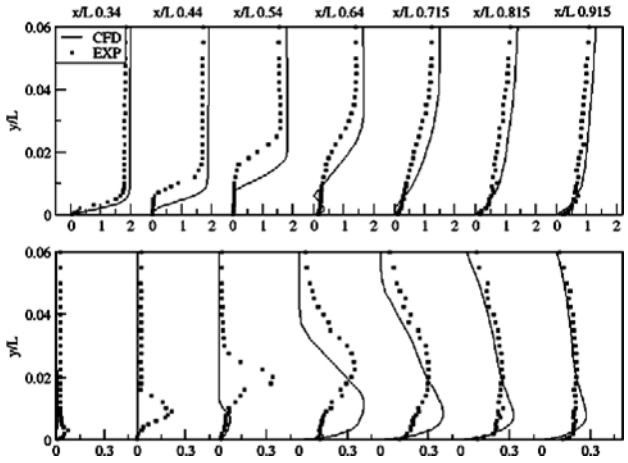

Fig. 9 Time-mean velocity U/U_{in} (top) and rms U/U_{in} (bottom) profiles (Re = 70,000, Uncontrolled).

shear layer rollup phenomenon that induces vortex shedding. In fact, the large velocity fluctuations occurring inside the separated shear layer are due not only to the turbulence activity, but principally to the large scale coherent vortical structures growing as a consequence of the shear layer rollup phenomenon that induces vortex shedding, as described in the work by Simoni *et al.* [17]. The large velocity fluctuations occurring inside the separated shear layer are not only due to the turbulence activity, but mainly to the large scale coherent vortical structures growing as a consequence of the boundary layer instability [14]. At x/L = 0.64 turbulence appears in the close to the wall region as a consequence of the shear layer transition process which transfers high momentum flow towards the wall thus inducing reattachment. The development of turbulent features as predicted by the RANS calculations is quite different. The much smaller turbulence intensity growth rate is connected to the different bubble height and overall structure of turbulent field inside the bubble. The three-equation turbulence model over-predicts the turbulence intensity near the wall ($x/L \approx 0.64$), as assessed in previous studies [15] whereas the turbulent kinetic energy peak value is under-predicted near the transition location ($x/L \approx 0.54$) at the edge of the separation bubble. As the momentum transfer is completed and the turbulent boundary layer establishes, the computed velocity and turbulent profiles appear in better agreement with the experimental ones. In conclusion, the separation induced transition mechanism is poorly described by the RANS simulations, although the final result and the extent of the transition process are correctly predicted.

Controlled condition

The boundary layer developing along the plate has also been surveyed with the synthetic jet installed. In Fig. 10 and Fig. 11 the experimental and numerical C_p distributions for Re = 70,000 and Re = 200,000 are reported for the different synthetic jet conditions (see Table 1).

For the smaller Reynolds number case (Fig. 10) the measured static pressure coefficient distribution for the smaller Strouhal number (St = 0.25, red dots) shows that the synthetic jet reduces separation extension but it is not able to completely prevent it, due to the very long and thick laminar bubble already documented for the steady uncontrolled condition. For this low Reynolds number case, the time-mean boundary layer laminar separation seems to be completely suppressed only for Strouhal numbers above 0.5.

The calculations are able to qualitatively predict the trend associated with the synthetic jet actuation frequency. Separation is reduced with increasing frequency, and it is completely suppressed at the highest Strouhal number. However, the predicted separation extension in the lowest Strouhal cases is even higher than that of the uncontrolled case. Apparently the separation onset moves downstream with increasing frequency. The exact position of the separation onset and its length are shown in Table 3 - as inferred from the numerical skin friction distribution, not reported here - and substantiate the previous observations.

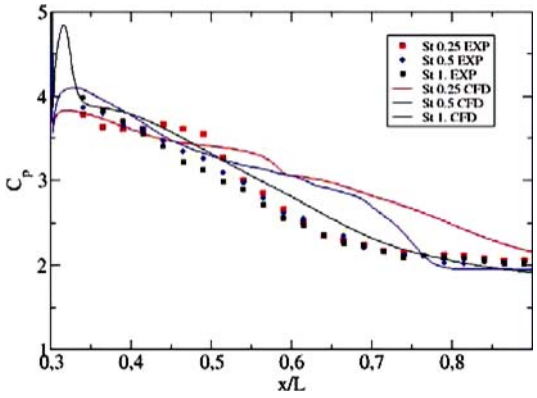

Fig. 10 Pressure coefficient distributions: Re = 70,000, controlled conditions.

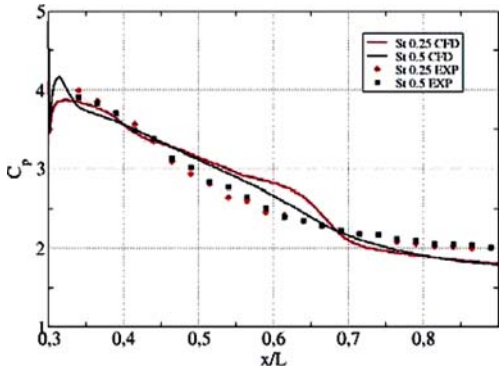

Fig. 11 Pressure coefficient distributions: Re = 200,000, controlled conditions.

For the highest Reynolds number case tested (Fig. 11), the small laminar separation bubble characterizing the uncontrolled condition appears in the experimental results completely suppressed by the jet even at the smallest Strouhal number (St = 0.25). For this Reynolds number an increase of the synthetic jet frequency does not introduce further benefits, since the separation bubble occurring in the uncontrolled case is already small. Thus, the higher energy expenditure requested to produce the jet with a Strouhal number larger than 0.25 seems wasted. This feature suggests that the additional momentum introduced in the boundary layer by the synthetic jet to prevent the laminar separation should be reduced when the Reynolds number increases because of the separation bubble length reduction.

The same positive trend with increasing Strouhal and amplitude is again qualitatively well predicted by the computations, but still large errors appear in the absolute value prediction. In the St = 0.25 case the jet reduces the separation extension and delays its onset, without suppressing it in a time-averaged sense. At St = 0.5 the plateau in the C_p distribution disappears indicating a stronger intervention of the jet in the boundary layer development. Actually separation seems prevented in a time-averaged sense, as displayed in Table 3.

In order to provide a detailed view of the synthetic jet effects, time-mean velocity and turbulence intensity profiles are shown in Fig. 12 for the smaller Reynolds number tested for the case St = 0.5, where the experimental static pressure coefficient distribution showed separation suppression. Experimental results of Fig. 12 confirm that in this case the synthetic jet is able to completely suppress in a time-averaged sense the large laminar separation bubble which occurs under the uncontrolled condition. Not only the velocity magnitude is reduced close to the wall from x/L = 0.34 up to x/L = 0.54, but also the zero velocity gradient in the normal to the wall direction

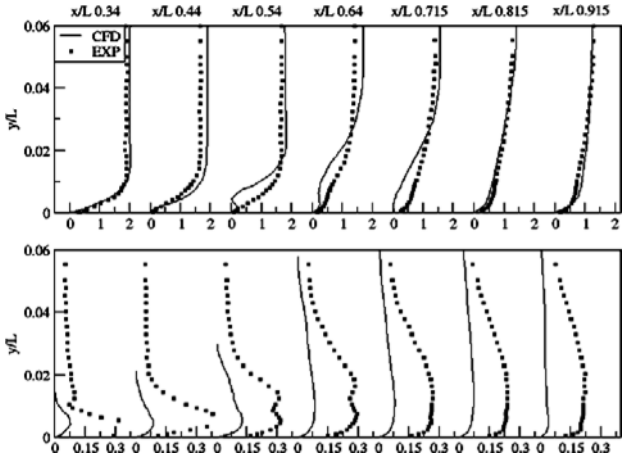

Fig. 12 Time-mean velocity U/Uin (top) and rmsU/Uin profiles (bottom) (Re = 70,000, St = 0.5).

has not been observed. Time-mean transition seems to begin downstream of x/L = 0.54, as suggested by the higher momentum characterizing the velocity profiles in the near wall region downstream of this position.

The large turbulence intensity magnitude observed in the first traverses is due to both periodic oscillations induced by the synthetic jet functioning and turbulence ejected by the jet during the blowing phase, as described in detail in Lengani et al. [16], where phase-locked measurements have been presented. These two effects help to increase the mixing process within the boundary layer avoiding separation.

The numerical streamwise velocity profiles highlight a small difference in the outer velocity magnitude at $x/L \approx$ 0.44, a fact already appreciated while discussing the C_p distribution. Upstream of separation onset the simulations under-predict the turbulence intensity both inside and outside the boundary layer. The latter can be ascribed to overestimated turbulence decay in the accelerating part of the nozzle. The low near-wall turbulence intensity in the first traverses indicates that simulations do not correctly predict the interaction between boundary layer and forced perturbation. These two discrepancies result in the lack of complete separation suppression which is recognizable at x/L = 0.54. As the flow reattaches, the normal to the wall velocity gradient is nearly zero up to $x/L \approx$ 0.715. At x/L = 0.815 a fully turbulent boundary layer profile seems to be recovered, although the momentum thickness is slightly higher than that in the experiments. The turbulence intensity magnitude is indeed also under predicted after reattachment.

Table 2 Separation position and extent, Re = 70,000

	x_{sep}/L		L_{sep}/L	
	EXP	CFD	EXP	CFD
Uncontrolled	0.395	0.435	0.295	0.295
St = 0.25	0.400	0.439	0.145	0.396
St = 0.5	-	0.458	-	0.312
St = 1	-	-	-	-

Table 3 Separation position and extent, Re = 200,000

	x_{sep}/L		L_{sep}/L	
	EXP	CFD	EXP	CFD
Uncontrolled	0.39	0.40	0.10	0.19
St = 0.25	-	0.64	-	0.04
St = 0.5	-	-	-	-

The numerical model actually misses the experimentally observed positive effect of the synthetic jet at lower frequency. This is in accordance with the behavior of the k -k_L-ω model, as documented in previous studies [12], showing prediction of transition location with an error of about 20% where an adverse pressure gradient exists. It

is therefore very difficult for the model to correctly represent the effect of an unsteady oscillation on the transition onset, from which flow separation inception and reattachment strongly depends. The effects of a high momentum thin layer of fluid injected in the boundary layer at higher frequencies and amplitudes is instead better predicted by the URANS model.

For the sake of a quantitative comparison, the separation position as well as its length obtained both experimentally and numerically are summarized in Table 2 and Table 3 for the two Reynolds numbers.

Conclusions

The effects of a synthetic jet with zero net massflow on a separated boundary layer have been investigated both experimentally and numerically. The adopted test-case deals with the flow over a flat plate subject to a favourable-adverse pressure gradient typically occurring on the suction side of high-lift low-pressure turbine blades.

Experiments have been undertaken in the low-speed wind tunnel at two different Reynolds numbers. The synthetic jet has been documented to be effective for both configurations in suppressing or reducing the separation in a time-averaged sense. At the higher Reynolds number a short separation appears in the uncontrolled case, and the synthetic jet lowest frequency and amplitude are sufficient for its suppression. At the lower Reynolds number a larger external energy supply is needed for the complete separation suppression; thus higher frequencies and amplitudes are required.

Numerical results obtained with a three-equation eddy viscosity model are shown to be able to qualitatively predict the overall effects of the synthetic jet. However the quantitative behaviour is often incorrect. Difficulties are also inherently associated with the selected test-case. The uncertainties on the unsteady behaviour of upper wall separation do affect the flat plate boundary layer development so much so that the prediction of even the uncontrolled condition is troublesome. Moreover, the turbulence model inherent limitations seem to constrain the ability to correctly capture unsteady transition onset, and therefore the interaction between synthetic jet perturbation and boundary layer development.

Acknowledgement

The support of the Italian Ministry of the University and Scientific Research (MIUR) under the PRIN project number 2007R3AXLH is greatly acknowledged.

References

[1] Honohan A. M., Amitay, M., Glezer A., Aerodynamic Control Using Synthetic Jets, AIAA Paper AIAA-2000-2401, Denver, CO, USA,(2000).

[2] You D., Moin P., Study of Flow Separation over an Airfoil with Synthetic Jet Control Using Large-Eddy Simulation, Technical report, Center for Turbulence Research, Stanford, CA, USA, Annual Research Brief, (2007).

[3] Volino R. J., Separation Control on Low-Pressure Turbine Airfoils Using Synthetic Vortex Generator Jets, Journal of Turbomachinery, vol. 125, pp. 765–777, (2003).

[4] Vera M., Zhang X. F., Hodson H., Harvey N., Separation and Transition Control on an Aft-Loaded Ultra-High-Lift LP Turbine Blade at Low Reynolds Numbers: High-Speed Validation, Journal of Turbomachinery, vol. 129, pp. 340–347, (2007).

[5] Rizzetta D.P., Visbal M.R., Numerical Study of Active Flow Control for a Transitional Highly-Loaded Low Pressure Turbine, Journal of Fluids Engineering, vol. 128, pp. 956–967, (2006).

[6] Rumsey C. L., Swanson R.C., Turbulence Modeling for Active Flow Control Applications, International Journal of Computational Fluid Dynamics, vol. 23, pp. 317–326, (2009).

[7] Dejoan A., Jang Y.-J., Leschziner M.A., Comparative LES and Unsteady RANS Computations for a Periodically Perturbed Separated Flow over a Backward-Facing Step, Journal of Fluids Engineering, vol. 127, pp. 872–878, (2005).

[8] Bernardini C., Carnevale M., Manna M., Martelli F., Features of Transition Mechanism by Synthetic Jet in a Low Pressure Turbine Decelerating Boundary Layer, Proceedings of 9th European Turbomachinery Conference, Istanbul, (2011).

[9] Gilarranz, J. L., Rediniotis, O. K., Compact, High-Power Synthetic Jet Actuators for Flow Separation Control, AIAA paper AIAA-2001-0737, Reno, NV, USA, (2001).

[10] Menter F.R., Langry R., Volker S., Transition Modelling for General Purpose CFD Code, Flow, Turbulence and Combustion, vol. 77, pp. 277–303, (2006).

[11] Menter F.R., Improved Two Equation k-ω Turbulence Models for Aerodynamic Flows, Technical Report, NASA Technical Memorandum 103978, (1992).

[12] Walters K. D-, Cokljat D., A Three-Equation Eddy-Viscosity Model for Reynolds-Averaged Navier-Stokes Simulations of Transitional Flows, Journal of Fluids Engineering, vol. 130, pp. 121401.1-121401.14, (2008).

[13] Cutrone, L., De Palma P., Pascazio G., Napolitano M., An Evaluation of Bypass Transition Models for Turbomachinery Flows, International Journal of Heat and Fluid Flow, vol. 28, pp. 161–177, (2008).

[14] Lengani, D. Simoni, D, Ubaldi, M., Zunino, P., Bertini, F., An Experimental Study of the Reynolds Number Influence on a Laminar Separation Bubble, ERCOFTAC Bulletin, vol. 80, pp. 24–29, (2009).

[15] Cutrone, L., De Palma P., Pascazio G., Napolitano M., Predicting Transition in Two- and Three-Dimensional Separated Flows, International Journal of Heat and Fluid Flow, vol. 29, pp. 504–526, (2008).

[16] Lengani, D. Simoni, D, Ubaldi, M., Zunino, P., Bertini, F., Application of a Synthetic Jet to Control Boundary Layer Separation under Ultra-High-Lift Turbine Pressure Distribution, Flow, Turbulence and Combustion, vol. 87, pp. 597–616, (2011).

[17] Simoni, D., Ubaldi, M., Zunino, P., Lengani, D., Bertini, F., An Experimental Investigation of the Separated-Flow Transition Under High-Lift Turbine Blade Pressure Gradients, Flow, Turbulence and Combustion, vol. 88, pp. 45–62, (2011).